HAL
open science

Physical and functional interplay between PCNA DNA clamp and Mre11–Rad50 complex from the archaeon Pyrococcus furiosus

Gaëlle Hogrel, Yang Lu, Sébastien Laurent, Etienne Henry, Clarisse Etienne, Duy khanh Phung, Rémi Dulermo, Audrey Bossé, Pierre-François Pluchon, Béatrice Clouet-D'orval, et al.

To cite this version:

Gaëlle Hogrel, Yang Lu, Sébastien Laurent, Etienne Henry, Clarisse Etienne, et al.. Physical and functional interplay between PCNA DNA clamp and Mre11–Rad50 complex from the archaeon Pyrococcus furiosus. Nucleic Acids Research, 2018, 46 (11), pp.5651-5663. 10.1093/nar/gky322 . hal-02390072

HAL Id: hal-02390072

https://hal.science/hal-02390072v1

Submitted on 9 Dec 2020

HAL is a multi-disciplinary open access archive for the deposit and dissemination of scientific research documents, whether they are published or not. The documents may come from teaching and research institutions in France or abroad, or from public or private research centers.

L'archive ouverte pluridisciplinaire **HAL**, est destinée au dépôt et à la diffusion de documents scientifiques de niveau recherche, publiés ou non, émanant des établissements d'enseignement et de recherche français ou étrangers, des laboratoires publics ou privés.

Distributed under a Creative Commons Attribution - NonCommercial 4.0 International License

Published online 8 May 2018 *Nucleic Acids Research, 2018, Vol. 46, No. 11* **5651–5663**
doi: 10.1093/nar/gky322

Physical and functional interplay between PCNA DNA clamp and Mre11–Rad50 complex from the archaeon *Pyrococcus furiosus*

Gaëlle Hogrel[1,2,3,†], Yang Lu[1,2,3,†], Sébastien Laurent[1,2,3], Etienne Henry[1,2,3], Clarisse Etienne[4], Duy Khanh Phung[4], Rémi Dulermo[1,2,3], Audrey Bossé[1,2,3], Pierre-François Pluchon[1,2,3], Béatrice Clouet-d'Orval[4] and Didier Flament[1,2,3,*]

[1]Ifremer, UMR6197, Laboratoire de Microbiologie des Environnements Extrêmes, 29280 Plouzané, France, [2]Université de Bretagne Occidentale, UMR6197, Laboratoire de Microbiologie des Environnements Extrêmes, 29280 Plouzané, France, [3]CNRS, UMR6197, Laboratoire de Microbiologie des Environnements Extrêmes, 29280 Plouzané, France and [4]Université de Toulouse; UPS, 118 Route de Narbonne, F-31062 Toulouse, France; CNRS; LMGM; F-31062 Toulouse, France

Received January 12, 2017; Revised April 11, 2018; Editorial Decision April 12, 2018; Accepted April 18, 2018

ABSTRACT

Several archaeal species prevalent in extreme environments are particularly exposed to factors likely to cause DNA damages. These include hyperthermophilic archaea (HA), living at temperatures >70°C, which arguably have efficient strategies and robust genome guardians to repair DNA damage threatening their genome integrity. In contrast to Eukarya and other archaea, homologous recombination appears to be a vital pathway in HA, and the Mre11–Rad50 complex exerts a broad influence on the initiation of this DNA damage response process. In a previous study, we identified a physical association between the Proliferating Cell Nuclear Antigen (PCNA) and the Mre11–Rad50 (MR) complex. Here, by performing co-immunoprecipitation and SPR analyses, we identified a short motif in the C- terminal portion of *Pyrococcus furiosus* Mre11 involved in the interaction with PCNA. Through this work, we revealed a PCNA-interaction motif corresponding to a variation on the PIP motif theme which is conserved among Mre11 sequences of Thermococcale species. Additionally, we demonstrated functional interplay *in vitro* between *P. furiosus* PCNA and MR enzymatic functions in the DNA end resection process. At physiological ionic strength, PCNA stimulates MR nuclease activities for DNA end resection and promotes an endonucleolytic incision proximal to the 5′ strand of double strand DNA break.

INTRODUCTION

Extremophile organisms provide remarkable study systems for understanding cellular processes that allow them to live in conditions likely to cause a high rate of DNA damage. Several archaeal species prevalent in extreme environments are particularly exposed to such stressors, including hyperthermophilic archaea (HA) living at temperatures >70°C. However, several studies have shown that HA such as *Pyrococcus furiosus and Sulfolobus solfataricus* can fully restore their genomes if they are fragmented by γ-radiation (1–3). They arguably have efficient strategies and robust genome guardians to repair DNA damage threatening genome integrity. These guardians are proteins working and interacting together in a carefully orchestrated ballet. Archaea employ 'eukaryotic' DNA replication and repair complex proteins (4), but several DNA repair protein families that are broadly conserved among Bacteria and Eukarya have not been found in Archaea (5). Using *in silico*, genetic or biochemical approaches, several studies revealed new actors or new complexes involved in genomic integrity in Archaea (6–15), leading to the characterization of new helicases and nucleases, like Hel308/Hjm, GAN, NucS/EndoMS and more recently NerA, thus, improving our understanding of genomic maintenance processes in Archaea. To contribute to this effort to discover new actors or new complexes involved in archaeal genomic integrity, we characterized a protein-protein interaction network sustaining genome maintenance in *Pyrococcus abyssi* (15). In this previous study, we identified a physical association between the Proliferating Cell Nuclear Antigen (PCNA) and the Mre11–Rad50 (MR) complex: the characterization of this association is addressed in the present study.

*To whom correspondence should be addressed. Tel: +33 298 224 527; Email: dflament@ifremer.fr
† The authors wish it to be known that, in their opinion, the two first authors should be regarded as joint First Authors.

© The Author(s) 2018. Published by Oxford University Press on behalf of Nucleic Acids Research.
This is an Open Access article distributed under the terms of the Creative Commons Attribution Non-Commercial License (http://creativecommons.org/licenses/by-nc/4.0/), which permits non-commercial re-use, distribution, and reproduction in any medium, provided the original work is properly cited. For commercial re-use, please contact journals.permissions@oup.com

Downloaded from https://academic.oup.com/nar/article-abstract/46/11/5651/4993783
by INIST-CNRS BiblioVie user
on 06 August 2018

Structurally conserved between Archaea and Eukarya, PCNA is a multimeric, ring-shaped factor that encircles DNA duplex. Archaeal Replication Factor C complex (RFC), which functions as a clamp loader, stimulates PCNA assembly around DNA even though archaeal PCNA can spontaneously load *in vitro* onto DNA (16,17). First reported as a processivity factor for DNA polymerases, PCNA is essential for cell viability. As a DNA-clamp, PCNA is a moving platform for numerous partners involved in DNA replication and repair pathways (18). Extensive lists of PCNA partners have been given in reviews (19–21).

The MR complex has a broad influence on the DNA damage response network, especially on repair of DNA Double-Strand Breaks (DSB) (22). As DSBs are a particularly threatening type of DNA damage, induced by external agents as well as by internal molecular events, cells have evolved a highly sophisticated DNA damage response system. For the recognition and repair of DNA breaks, the two major mechanisms are Homologous Recombination (HR) and Non-Homologous End-Joining (NHEJ). In HR, the broken ends are resected into 3′ single-strand tails and then used as templates for a homology search; whereas in NHEJ, the broken ends are directly rejoined (for reviews see (23–25)). In Eukarya, DSBs are repaired by either HR or NHEJ depending on the cell cycle (26). NHEJ was assumed to be absent from Archaea until Bartlett *et al*. reconstituted an archaeal NHEJ apparatus *in vitro* similar to that of bacterial machinery (27). In contrast to eukaryotes and other archaea, HR appears to be a vital pathway in HA, since genetic analyses have shown that the *mre11*, *rad50* and *radA* genes are essential for *Thermococcus kodakaraensis* and *Sulfolobus islandicus* (28,29).

The eukaryotic macromolecular machine MR(N/X) is composed of two core proteins, Mre11 and Rad50, with an additional component: Nbs1 for higher eukaryote or Xrs2 for yeast, which are found in neither Bacteria nor Archaea. Both Mre11 and Rad50 are highly conserved in all three domains and even exist as gp46/47 in some virus such as T4 phage (30). The MR complex engages the HR pathway by tethering and resecting DNA ends through a combination of nuclease and ATPase activities tightly related to conformational changes (31). However, the MR complex nuclease functions, 3′→5′ double strand (ds) DNA exonuclease activity and single strand (ss) DNA endonuclease activity, are not sufficient to generate a long 3′ ssDNA tail and require additional partners to catalyse efficient DSB resection (32). Moreover, the MR complex appears to be essential in replication fork restart in eukaryote cells, but to date the biochemical and regulation mechanisms remain partially understood.

Given the role of PCNA to orchestrate DNA replication and other DNA processes, we wondered whether this newly discovered interaction with the MR complex would regulate MR enzymatic functions in the DNA end resection process. By performing co-immunoprecipitation and SPR analyses, we demonstrated physical association between *P. furiosus (Pfu)* PCNA and the MR complex and identified a short motif in the C terminal portion of *Pfu*Mre11 that interacts with *Pfu*PCNA and corresponds to a variation on the PCNA-Interaction Peptide (PIP) motif theme. Enzymatic assays, at physiological ionic strength, showed that *Pfu*PCNA stimulates nuclease activity of the *Pfu*MR complex on dsDNA substrates and promotes an endonucleolytic incision proximal to the 5′ strand of a DNA double strand break in a manner still consistent with HR process requirements.

MATERIALS AND METHODS

Proteins and peptides

A gene coding for *P. furiosus* PCNA was inserted into pET19b to add an N-terminal 10xHis-tag (plasmid provided by B. Connolly (33)) and expressed in *Escherichia coli* Rosetta pLysS. The *P. furiosus* MR complex was co-expressed from a bicistronic pET27b vector (gift from J. Tainer and T. Paull (34)) in BL21 DE3 codonplus *E. coli* adding a 6xHis-tag in the N-terminal region of Mre11. This *P. furiosus Mre11–Rad50* plasmid was used to build a *P. furiosus Mre11–Rad50 ΔPIP* mutant (1–411) using Q5® Site-Directed Mutagenesis Kit (BioLabs). *P. furiosus* Mre11–Rad50^{link1}, Rad50^{link2} and Mre11^{core} proteins were provided by G. Williams and J. Tainer.

Cells were grown at 37°C to an OD_{600} 0.7–0.8, and expression was induced by addition of 1 mM IPTG (final concentration). Four hours after induction, cells were harvested by centrifugation and re-suspended in a buffer containing (i) for *Pfu*PCNA proteins: 10 mM Tris–HCl pH 7.4, 500 mM NaCl, 20 mM imidazole, 1 mM DTT, (ii) for *Pfu*MR wt and *Pfu*MR ΔPIP: 20 mM Tris–HCl pH 8.0, 500 mM NaCl, 10 mM imidazole, 1 mM DTT, supplemented by EDTA-free protease inhibitor (Roche). Cells were lysed by applying 1.9 kbar pressure (One shot, Constant Systems). *Pfu*PCNA, *Pfu*MR wt and ΔPIP supernatants were incubated overnight with DNase I at 37°C and then heated at 75–80°C for 20 min. After centrifugation, soluble fractions were loaded onto a HisPrepFF 16/10 (GE Healthcare) nickel resin column. After a wash step, elution was performed with a linear gradient from 10 to 500 mM imidazole. Peak fractions were run on 15% SDS-PAGE gels (Bio-Rad), then pooled and concentrated using Vivaspin columns (10 or 30 MWCO) before running on a Superdex 200 10/300 GL column (GE Healthcare). *Pfu*PCNA was eluted in 10 mM Tris–HCl pH 7.4, 200 mM NaCl, 1 mM DTT and *Pfu*MR wt and ΔPIP in 20 mM Tris–HCl pH 8.0, 150 mM NaCl, 1 mM DTT complemented with 20% glycerol and stored at −20°C. Proteins were quantitated using DC protein assay (BioRad) for *Pfu*PCNA, and absorbance measurement at 280 nm for *Pfu*MR wt and ΔPIP complexes. All molar concentrations indicated in this study corresponded to the homotrimeric PCNA and to the heterotetrameric form of the M_2R_2 complex.

Peptides to be used as competitors for PCNA-binding in pull-down assays were synthesized and purified (>90% purity) by Genepep (St-Jean-de-Védas, France). The PIP-like Mre11 peptide was derived from the *Pfu*Mre11 sequence (412–424): Ac-KKKRGTLDSWLGG-NH_2. The peptide used as the negative control (PIP–) was: Ac-KEVKEEYKRFLEE-NH_2 (12).

Downloaded from https://academic.oup.com/nar/article-abstract/46/11/5651/4993783
by INIST-CNRS BiblioVie user
on 06 August 2018

Co-immunoprecipitation experiments

To study the physical interaction between *Pfu*PCNA and *Pfu*MR wt or ΔPIP, 8.33 μg of anti-*P. abyssi* (*Pab*) PCNA polyclonal antibody was immobilized onto 1.5 mg of magnetic Dynabeads Protein A (ThermoFischer). Subsequently, antibodies were covalently anchored using 57 μg of BS3 crosslinker (Thermo Scientific); such an amount of beads was determined in order to specifically bind 1 μg of *Pfu*PCNA input (data not shown). In a 20 μl reaction volume, 1 μg *Pfu*PCNA was incubated for 30 min at 4°C with 10 μg *Pfu*MR wt or ΔPIP complexes in binding buffer (25 mM HEPES pH 7.0, 150 mM NaCl, 1 mM DTT, 0.05% Tween 20). The resulting protein complexes were trapped by anti-PCNA Dynabeads over 10 min at 4°C. Beads were washed three times with binding buffer (100 μl) before final elution for 10 min at 95°C in denaturating XT loading buffer (Bio-Rad). Proteins were then separated on SDS-PAGE (4–20% Pierce) and visualized using Coomassie Blue dye. Pull-down assays were performed following the same procedure for the three *Pfu*MR constructs, with the exception that protein complexes were formed during 1 h at 4°C and incubated with the bead-antibody complex for 5 min at 4°C and then washed three times at 25°C. A 1:3 molar ratio *Pfu*PCNA:*Pfu*MR proteins was used. As input controls, 1 μg of proteins was loaded onto SDS-PAGE.

For co-immunoprecipitation experiments in presence of PIP-like peptide, in 20 μl reaction, 1 μg *Pfu*PCNA was incubated with a 100 molar excess of competitor peptide or negative control peptide at least 1 h at 4°C in binding buffer. Then, 10 μg *Pfu*MR complex was added to the PCNA/peptide solution for 5 min at 4°C. The resulting protein complexes were trapped by anti-PCNA Dynabeads, washed three times with 50 μl binding buffer at 4°C and eluted as described above. After SDS-PAGE separation, proteins were transferred onto a PVDF membrane (Thermo Scientific). *Pfu*PCNA and *Pfu*Mre11 were simultaneously probed using anti-His monoclonal antibody (Invitrogen). Proteins were revealed by immunofluorescence using an ECL 2 blot kit (Thermo Scientific). Image acquisition was done with a ChemiDoc XRS+ (BioRad) and quantifications carried out using QuantityOne software (Bio-Rad).

DNA substrates

Oligonucleotides were purchased from Eurogentec and purified by RP-HPLC for S50/50, S50/50s, S50s/50s, S87/87s and S87s/87s or by PAGE for substrates containing reporter-quencher pairs, RQ-S87s/87s and RQ23-S87s/87s (Sequences in supplementary data). DNA substrates were annealed, at a 1:1 primer:template ratio, in presence of 10 mM HEPES pH 7.5 and 100 mM NaCl by heating at 95°C for 5 min and cooling to room temperature.

Nuclease assays

Nuclease activities of *Pfu*MR wt and ΔPIP complexes on linear dsDNA substrates was followed in 10 μl reactions containing 25 nM DNA in 25 mM HEPES pH 7.0, 1 mM DTT, 0.5 mg/ml BSA complemented with 1 mM ATP, 5 mM $MgCl_2$, 5 mM $MnCl_2$ and 150 or 300 mM NaCl, as indicated in the figure captions. Pre-incubation was performed with 25 nM dsDNA substrates and the indicated concentrations of *Pfu*PCNA at ambient temperature for 5 min followed by an incubation with the indicated concentrations of *Pfu*MR wt or ΔPIP complexes at 70°C for different times as indicated in the figures. Reactions were stopped by addition of 85% deionized formamide, 0.01 N NaOH, 10 mM EDTA, 2 μM Trap (RC50 or RC87) and by heating samples at 95°C for 5 min. DNA products were separated by electrophoresis on a gel composed of 15% or 18% polyacrylamide 19:1, 7 M urea, 16% deionized formamide and 1× Tris Borate EDTA (TBE). Labeled fragments were analysed with a fluorimager Typhoon 9500 (GE Healthcare) and quantified with Image Quant software.

Real time fluorescence DNA unwinding assays

Unwinding assays were carried out at 55°C using dsDNA RQ-S87s/87s and RQ23-S87s/87s, which contain a fluorophore-quencher pair (6-FAM, 6-carboxyfluorescein/DDQI, Deep Dark Quencher I or BHQ-1, Black Hole Quencher 1) positioned at the DNA end or 23 nt from the extremity. Emission of fluorescence was triggered by unwinding quenched DNA duplex substrates. Unwinding assays were performed in 50 μl of 25 mM HEPES pH 7.0 buffer containing 25 nM DNA, 300 mM NaCl, 1 mM DTT, 0.5 mg/ml BSA, 5 mM $MgCl_2$ and 500 nM Trap 3′ 87RC, complemented with 1 mM ATP and 5 mM $MnCl_2$ when indicated. 50 nM *Pfu*PCNA were pre-incubated with the DNA mix for 5 min at ambient temperature before adding 25 nM *Pfu*MR wt or ΔPIP. Fluorescence emission was monitored using Q-PCR equipment (StepOnePlus™ Real Time PCR System Thermo Fisher Scientific). After 30 min, the temperature was increased to 95°C to induce complete unwinding to determine the maximum fluorescence intensity (100% unwinding signal, Q_{max}).

Unwinding percentage was calculated as follows: Unwinding % $= \frac{Q}{(Q_{max} - Q_0)} \times 100$, where Q was the real-time detected fluorescence and Q_0 corresponds to the fluorescence measured at the beginning of the reaction. Unwinding assays were repeated at least three times.

SPR experiments

Data were obtained using a Reichert SR7000DC spectrometer instrument (Reichert Inc., Buffalo, NY, USA). The running buffer was 25 mM HEPES pH 7.0, 300 mM NaCl, 1 mM DTT and 0.05% Tween 20, and flow rate was 25 μl/min. *Pfu*PCNA was immobilized on a mixed self-assembled monolayer (10% C11-(OEG)6-COOH: 90% C11-(OEG)3-OH), Reichert Inc.) via classic amine coupling chemistry and 25 nM of *Pfu*MR wt or ΔPIP complexes were injected over the *Pfu*PCNA surface at 25°C. The chip was regenerated after serial injections of 100 mM H_3PO_4 (3 × 30 s). Each curve displayed was double referenced with a set of blank buffer injections.

Downloaded from https://academic.oup.com/nar/article-abstract/46/11/5651/4993783
by INIST-CNRS BiblioVie user
on 06 August 2018

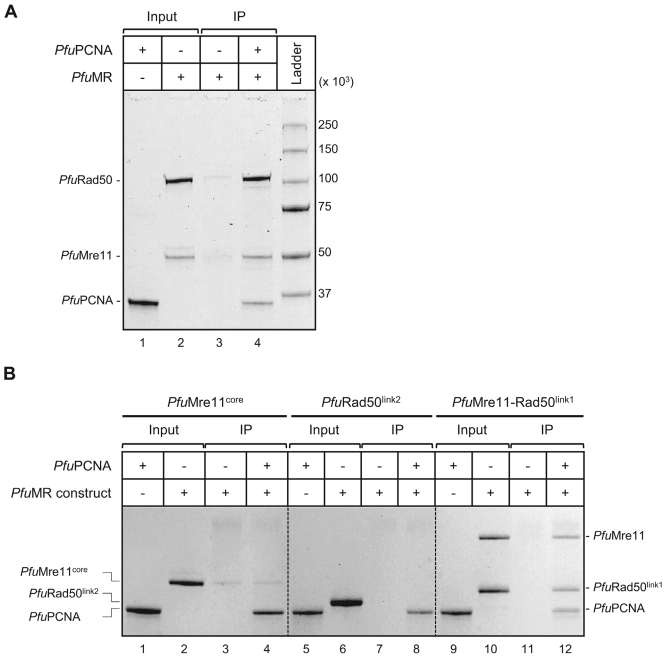

Figure 1. Physical association of *P. furiosus* PCNA and Mre11–Rad50. Protein-protein interactions were determined, *in vitro,* using a bead-based co-immunoprecipitation assay. (**A**) Full length *Pfu*MR co-immunoprecipitated with *Pfu*PCNA, (**B**) co-immunoprecipitation assays with *Pfu*PCNA and different *Pfu*Mre11 and *Pfu*Rad50 protein constructs (details given in Supplementary Figure S1B). 1 μg of protein was loaded on SDS-PAGE as Input. IP corresponds to the immunoprecipitation assays in presence of beads coated with PCNA antibodies. Fraction bound to the beads were analysed by Coomassie blue staining. Assays were performed in buffer with 150 mM NaCl.

RESULTS

P. furiosus PCNA physically interacts with the MR complex

We first considered using the homologous system with *P. abyssi* recombinant proteins but failed to achieve a proper level of production of the MR complex. As an alternative we used the recombinant proteins from the close species *Pyrococcus furiosus*. Complexes of *Pfu*PCNA and *Pfu*MR from *P. furiosus* were produced and purified (Supplementary Figure S1A). Using co-immunoprecipitation, we demonstrated that these two components also formed a complex in *P. furiosus*, as shown by the co-precipitation of the *Pfu*MR complex with *Pfu*PCNA (Figure 1A). We then explored some conditions where this association could take place. As illustrated in Supplementary Figure S1C, the complex could form in presence or absence of a metallic co-factor and ATP. As protein samples were DNA free after DNase I treatment, we assumed that the interaction between *Pfu*MR complex and *Pfu*PCNA is not dependent on DNA substrates.

To investigate the surface of interaction, we were able to use three *Pfu*Mre11 and *Pfu*Rad50 deletion constructs (35). *Pfu*Mre11^{core} (residues 1–342) lacks 84 C-terminal residues including its Rad50 binding domain (RBD); *Pfu*Rad50-link2, an untagged version of *Pfu*Rad50 with shortened coiled coils (unable to bind Mre11) connected by an intramolecular Gly-Gly-Ser-Gly-Gly sequence; and *Pfu*Mre11–Rad50-link1 a complex of another shortened version of *Pfu*Rad50 (able to bind Mre11 RBD) purified with full-length *Pfu*Mre11 (Supplementary Figure S1B). Only the *Pfu*Mre11–Rad50-link1 construct could form a complex with *Pfu*PCNA in solution (Figure 1B, compare lanes 4, 8 and 12). These data indicated that *Pfu*PCNA does not interact directly with *Pfu*Rad50 and that the coiled-coil domain of *Pfu*Rad50 is not required for recruitment of the MR complex onto *Pfu*PCNA. On the other hand, these observations raised two non-exclusive hypotheses: *Pfu*PCNA/MR interaction requires prior *Pfu*MR complex formation and/or is mediated by the C-terminal region of *Pfu*Mre11 absent in the Mre11^{core} construct. With the exception of a domain interacting with the base of *Pfu*Rad50's coiled-coils (348–381), the C-terminal domain of *Pfu*Mre11 is predicted to be disordered or flexible and is thought to be responsible for protein-protein and protein–DNA interactions (31).

The C-terminal region of *P. furiosus* Mre11 contains a putative PCNA interacting motif

PCNA-binding partners generally possess a PCNA-Interaction Peptide (PIP) motif, usually located at the extreme N- or C-terminus (36). The results obtained prompted us to look for a potential PIP motif at the C-terminal portion of *Pfu*Mre11. The core element of the archaeal PIP-box is a peptide with a sequence Qxxϕ (ϕ being hydrophobic residues L, M or I), which in most cases is C-terminally flanked by the sequence xxΩΩ (Ω being aromatic residues F or W) (37). Based on the alignment of PIP-Box like sequences (QXXϕXXΩΩ) from a subset of *Pyrococcus sp.* proteins whose affinity for PCNA has already been described (19), we identified a candidate PCNA-interacting peptide in the C-terminal region of *Pfu*Mre11 (Figure 2A). Located in the extreme C-terminal portion of *Pfu*Mre11 (positions 412–422) the motif exhibits the conserved hydrophobic residues but lacks the otherwise conserved glutamine residue. In addition, N-terminal extension from the motif is composed of a stretch of basic residues known to interact with the positively charged outer surface of PCNA (38). As Meslet-Cladiere *et al.* described, high affinity peptides for PCNA tend to be positively charged (12). Here the identified peptide has a predicted Isoelectric Point (p*I*) of 10.29 consistent with this property. 3D structure of the complete C-terminal Mre11 region has not been resolved to date; however, Hydrophobic Cluster Analysis identified this motif as a globular region and showed that the hydrophobic residues clustered with a similar shape to that observed for canonical PIP motif sequences (data not shown). Although this motif lacks the glutamine conserved residues, these features strongly suggest that it could act as a hydrophobic anchor on PCNA.

We then looked at occurrence of this motif in Mre11 sequences among species of the order Thermococcales. Remarkably, all available sequences displayed this putative PCNA-interacting motif in the C-terminal region (Supplementary Figure S2). From this alignment, we could derive a pattern [PK]-x-[KRNA]-x-[GSPNK]-x(1,3)-[IL]-x(2)-[WFY]-[ILV]) for a motif search using Scanprosite on archaeal protein sequences from Swiss-prot and

Downloaded from https://academic.oup.com/nar/article-abstract/46/11/5651/4993783
by INIST-CNRS BiblioVie user
on 06 August 2018

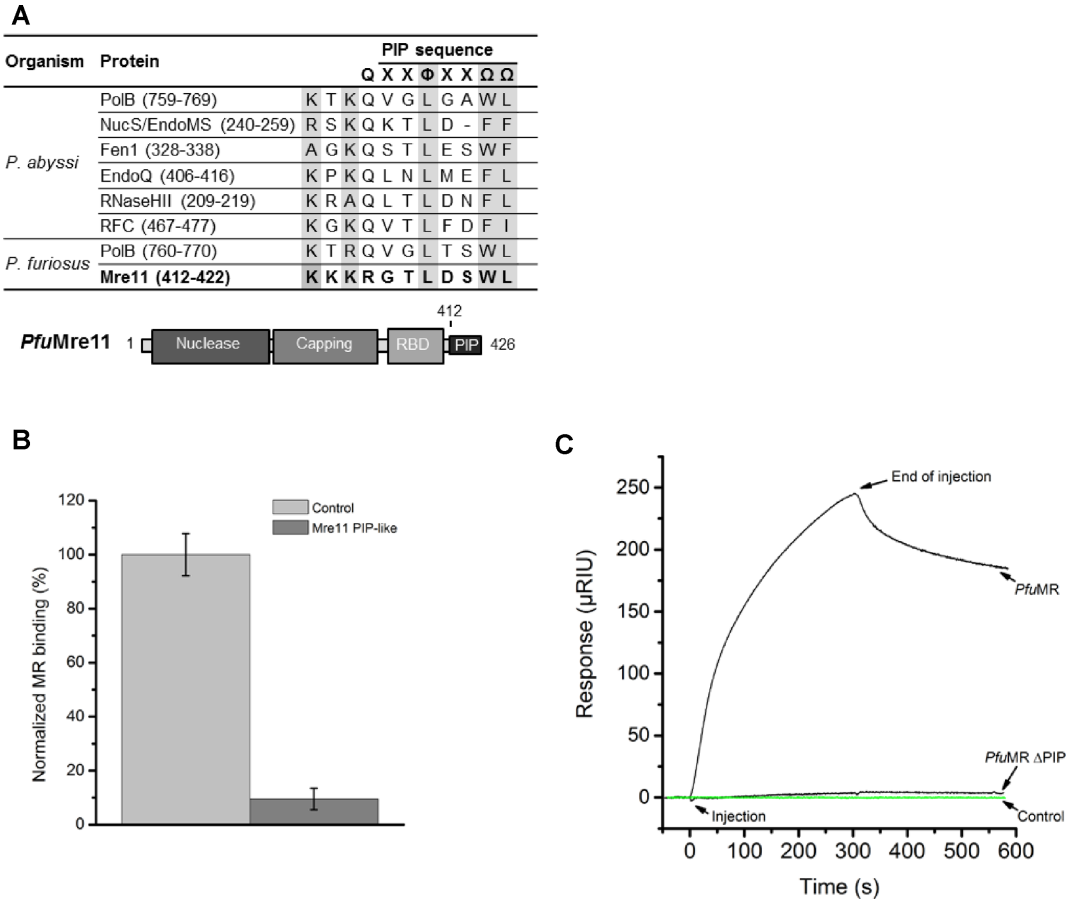

Figure 2. Identification of a putative PCNA binding motif in the C-terminal region of *Pfu*Mre11. (**A**) *Pfu*Mre11 displays a C-terminal PIP-like motif when compared with the consensus sequence (x, any residues; Φ, hydrophobic; Ω, aromatic or hydrophobic) and various sequences of proteins from *Pyrococcus sp.* known to interact with PCNA through the PIP motif. Positions within the sequences are indicated and *Pfu*Mre11 domains are illustrated below the table. (**B**) The interaction *Pfu*PCNA/MR is inhibited by an excess of Mre11 C-terminal peptide in competitive co-immunoprecipitation assays. Western blot signals of *Pfu*Mre11 were normalized with corresponding signals obtained with a peptide control. Experiments were performed in binding buffer containing 150 mM NaCl. Error bars represent standard deviation of three independent reactions. (**C**) Surface plasmon sensograms obtained after injection of 25 nM *Pfu*MR wt or ΔPIP over an immobilised *Pfu*PCNA surface. The running buffer contained 300 mM NaCl.

TrEMBL databases. This pattern was detected in Mre11 sequences from the order Thermococcales and from an Archeoglobale, *Archeoglobus fulgidus*. We also identified that Hel308/Hjm archaeal members of helicase superfamily 2 possessed a similar motif in the extreme C-terminal region (Supplementary Figure S2). Presence of this PIP-like motif in Hel308/Hjm sequences showed similar repartition as in sequences of Mre11, as only Thermococcale Hel308/Hjm helicases harboured the motif, with the exception of *Thermococcus litoralis*. In addition, alignment of the C-terminal region of Hel308/Hjm and Mre11 proteins showed a strong conservation of hydrophobic residues in the C-terminal extension of the motif (Supplementary Figure S2), suggesting that this structural element could also serve as a hydrophobic plug on PCNA surface. Most noticeably, interaction between PCNA and Hel308/Hjm from *P. furiosus* has already been described. Using a deletion mutant lacking the 20 residues at the extreme C-terminal region (39), the authors proposed that this portion could mediate interaction with PCNA which is consistent with our analysis.

Mre11 C-terminus region is essential for *Pfu*PCNA/MR interaction

Taken together, these observations prompted us to verify the assumption that the C-terminus of *Pfu*Mre11 contributes to *Pfu*PCNA/MR complex formation. To this aim, we performed pull-down competitive assays with the Mre11 peptide corresponding to the revealed motif (412-KKKRGTLDSWLGG-424). Figure 2B shows that an excess of the Mre11 peptide (Mre11 PIP-like) significantly blocked *Pfu*PCNA/MR interaction compared with the control peptide. As shown in the graph, the amount of immunoprecipitated Mre11 decreased drastically in the assay with the competitive peptide suggesting that this peptide inhibits assembly of the *Pfu*PCNA/MR complex. To test whether the C-terminal sequence of *Pfu*Mre11 could mediate interaction of the *Pfu*MR complex with *Pfu*PCNA, we used Surface Plasmon Resonance (SPR) with *Pfu*PCNA immobilized on a chip. SPR measurements indicated that the Mre11 peptide physically interacts with *Pfu*PCNA at a micromolar range of concentrations (Supplementary Fig-

Downloaded from https://academic.oup.com/nar/article-abstract/46/11/5651/4993783
by INIST-CNRS BiblioVie user
on 06 August 2018

ure S3A). It is interesting to note that the binding value (4.05 μM) correlates with K_D value obtained with a canonical PIP motif peptide derived from the sequence of another nuclease, *P. abyssi* NucS (40). Together, these results suggest that the primary docking site of *Pfu*Mre11 on *Pfu*PCNA could be similar to that described for PIP-motif containing proteins.

To confirm the essentiality of the PIP-like motif for the interaction, we produced a deleted version of the *Pfu*MR complex lacking the last 15 amino acids of the *Pfu*Mre11 subunit (Supplementary Figure S3B, left panel). The co-IP experiments clearly showed that the mutant *Pfu*MR ΔPIP complex did not bind to *Pfu*PCNA (Supplementary Figure S3B, right panel, compare lanes 4 and 10), providing conclusive evidence that this variation in the PIP motif mainly contributes to the interaction of the *Pfu*MR complex with *Pfu*PCNA. We then looked at the stability of the interaction at a higher salt condition to test specificity and to get closer to the reported physiological ionic strength of *Pyrococcus furiosus* (41). Supplementary Figure S3B indicates that the interaction between *Pfu*MR and *Pfu*PCNA is stable at 300 mM NaCl (lanes 5–6) and that the mutant *Pfu*MR ΔPIP complex did not interact with *Pfu*PCNA under the same conditions (lanes 11–12). As a final point on the physical interaction, the direct association between *Pfu*PCNA and the full length *Pfu*MR complex was confirmed by SPR analysis at 300 mM NaCl. *Pfu*MR specifically bound to *Pfu*PCNA anchored on a sensor chip, while the *Pfu*MR ΔPIP complex did not bind under the same conditions (Figure 2C). In addition, we conducted a kinetic experiment over the full range of *Pfu*MR complex concentrations and determined an apparent dissociation constant value (K_{Dapp}) of ∼4.07 ± 1.46 nM (Supplementary Figure S3C).

*Pfu*PCNA stimulates *Pfu*MR activity for dsDNA cleavage

In archaea, as in some other organisms, the MR complex is implicated in early steps of the HR pathway. Thanks to a combination of Mre11 nuclease and Rad50 ATPase activities, the MR complex initiates DNA end resection to provide suitable DNA template used by subsequent HR components. In several *in vitro* studies, *Pfu*Mre11 displayed distinct activities: 3′→5′ dsDNA exonuclease, ssDNA endonuclease and endonucleolytic cleavage on the 5′ strand at a break (30,34,42–44). Given PCNA preference for dsDNA substrate, we tested influence of the *Pfu*PCNA on *Pfu*MR complex nuclease activities to resect synthetic dsDNA oligonucleotides.

To this end, we performed nuclease assays on a linear blunt-end dsDNA substrate (S50/50s). The unlabeled complementary strand has phosphorothioate bonds at its 3′ end to block 3′→5′ exonuclease activity, in order to characterize exo- and endonuclease activities on the top strand irrespective of exonuclease degradation of the complementary strand (Figure 3A). We first confirmed that the nuclease activities of the *Pfu*MR complex were in accordance with previously reported activities at low salt conditions (Supplementary Figure S4A) and observed DNA products as already described on the same dsDNA substrates (42). Intracellular salt concentration was determined to be ∼350 mM in *P. furiosus* (41), we then decided to test the activity of the *Pfu*MR complex and impact of *Pfu*PCNA at 300 mM NaCl, close to the reported ionic strength. Increased concentrations of *Pfu*MR complex were incubated for 30 min at 70°C with dsDNA substrate. DNA fragments from the 5′-labeled strand was revealed by fluorescence (Figure 3B). As shown in lanes 6–7, the 5′-labeled strand was degraded by the *Pfu*MR complex, although to a much lesser extent than at low salt condition (compare with Supplementary Figure S4A), and defined products ranging from 15 to 37 nt were generated.

From a *Pfu*MR:DNA ratio of 1:1, conditions in which *Pfu*MR was inactive, we tested increased concentrations of *Pfu*PCNA and observed strong activation of DNA degradation activity (Figure 3C, lanes 7–9) with about 94% of the substrate used. Moreover, addition of *Pfu*PCNA, changed the degradation pattern and increased the specificity of the enzyme towards generation of major products ranging from 27 to 29 nucleotides (compare lanes 7 in Figure 3B and Figure 3C). A time course experiment confirmed that the products accumulated over time and were the major end products of the reaction (Supplementary Figure S4C). As expected, this activation was not observed in presence of the mutant *Pfu*MR ΔPIP (Figure 3D, compare lanes 3 and 5). To confirm that the interaction of *Pfu*PCNA with the *Pfu*MR complex is responsible of nuclease activation, we demonstrated that the ΔPIP mutant is not affected in its nuclease activity (compare Figure 3B and C with Supplementary Figure S4 D and E), indicating that direct interaction was necessary to stimulate *Pfu*MR nuclease activity. However, faint bands at 27–29 nt could still be observed on Figure 3D when *Pfu*MR ΔPIP was in presence of *Pfu*PCNA, indicating that the secondary domain of interaction might account for a weak resilient interaction with *Pfu*PCNA.

At 150 mM NaCl, we also a noticed change in the degradation pattern of DNA caused by *Pfu*PCNA, but this shift came with a strong inhibition of substrate utilization by *Pfu*MR, contrary to what was observed at 300 mM NaCl, and most importantly, we found no significant differences between *Pfu*MR wt and ΔPIP activities in presence of *Pfu*PCNA (Supplementary Figure S4B). These led us to test, for both salt concentrations, the ability of *Pfu*MR to bind dsDNA. By performing EMSA experiments, we confirmed its binding onto DNA at 150 and 300 mM NaCl and noticed no significant change caused by *Pfu*PCNA (Supplementary Figure S5), indicating that nuclease inhibition or activation effect was not due to an improvement or a blockage of *Pfu*MR fixation onto DNA substrates. This demonstrated the relevance of characterizing the functional interplay between *Pfu*MR and *Pfu*PCNA in higher salt concentration conditions than for previous reported characterizations of the MR complex from *P. furiosus*, especially as we were approaching physiological ionic strength with this treatment (41).

We also explored the effect of *Pfu*PCNA on metal dependence of nucleolytic degradation. Mre11 has two metal binding sites for which manganese has a higher affinity (43) whereas Rad50 needs magnesium to hydrolyse ATP (45). Supplementary Figure S6A showed that at 70°C, dsDNA

Downloaded from https://academic.oup.com/nar/article-abstract/46/11/5651/4993783
by INIST-CNRS BiblioVie user
on 06 August 2018

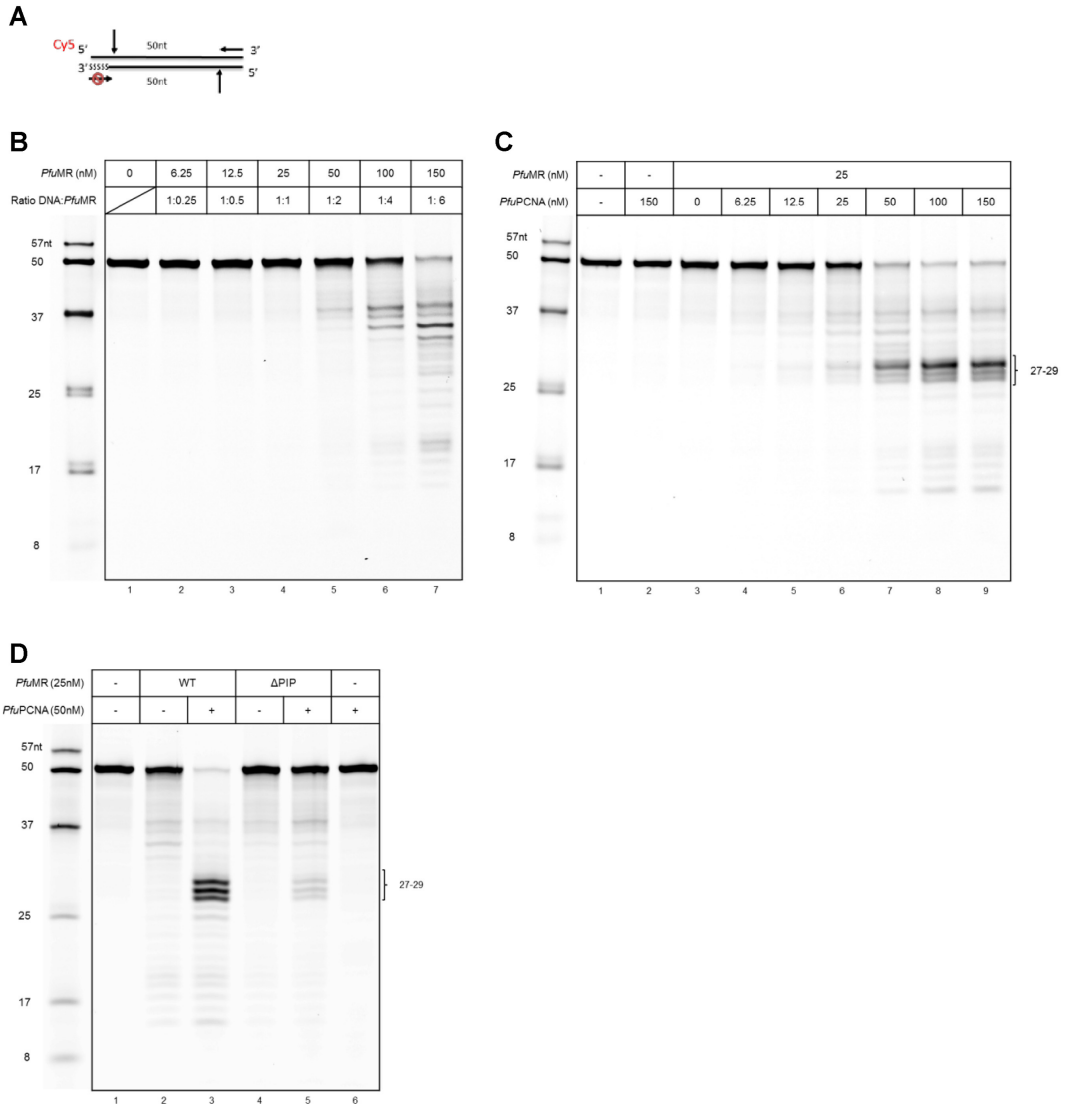

Figure 3. *Pfu*PCNA stimulates DNA degradation activity of *Pfu*MR. *In vitro* nuclease assays (**A**) 5′-labeled 50bp dsDNA substrate used. SSSSS represents phosphorothioate bonds. Black arrows indicate potential endo- and exo-nuclease cleavage activities. (**B**) 25 nM of DNA substrate were incubated at 70°C for 30 min with increasing concentrations of *Pfu*MR wt. (**C**) 25 nM of DNA substrate were pre-incubated with indicated concentrations of *Pfu*PCNA at room temperature for 5 min before adding 25 nM *Pfu*MR wt. Reactions were performed for 30 min at 70°C. (**D**) 25 nM of DNA substrate were pre-incubated with 50 nM *Pfu*PCNA at room temperature for 5 min before adding 25 nM *Pfu*MR wt or ΔPIP. Reactions were performed for 30 min at 70°C in 300 mM NaCl. DNA products were resolved in 18% PAGE and fluorescence revealed using Typhoon 9500 (GE Healthcare).

nucleolytic cleavage strongly required both ATP and manganese and that change in cleavage specificity observed in presence of *Pfu*PCNA was not dependent on the presence or absence of magnesium. Hereinafter we focus on our data obtained at 300 mM NaCl, with 10 mM ATP, 5 mM $MgCl_2$ and 5 mM $MnCl_2$ (similar results were obtained with KCl instead of NaCl, data not shown).

From the degradation pattern observed, it is tempting to speculate that this product occurred through endonucleolytic cleavage, which might be promoted upon association with *Pfu*PCNA. However, at this point it is not possible to conclude whether *Pfu*PCNA had an effect on the exonuclease, the endonuclease or regulated both activities of the *Pfu*MR complex.

Cleavage of the 5′-terminated DNA strand is promoted by *Pfu*PCNA/MR association

To address this question, we used dsDNA substrates protected against exonuclease activity at both 3′ ends (S50s/50s), which consequently could be only degraded by endonuclease activity. As observed previously, major DNA products of 27–29 nt were generated from blocked 3′ end substrate (Figure 4A), confirming that the pattern observed stems from the initial endonuclease cut. To question whether phosphorothioates bonds in synthetic oligonucleotides may have an impact on *Pfu*PCNA effect, we used unprotected blunt dsDNA substrate. Supplementary Figure S7A clearly shows that addition of *Pfu*PCNA generated a similar change of cleavage specificity in that it led to the

Downloaded from https://academic.oup.com/nar/article-abstract/46/11/5651/4993783
by INIST-CNRS BiblioVie user
on 06 August 2018

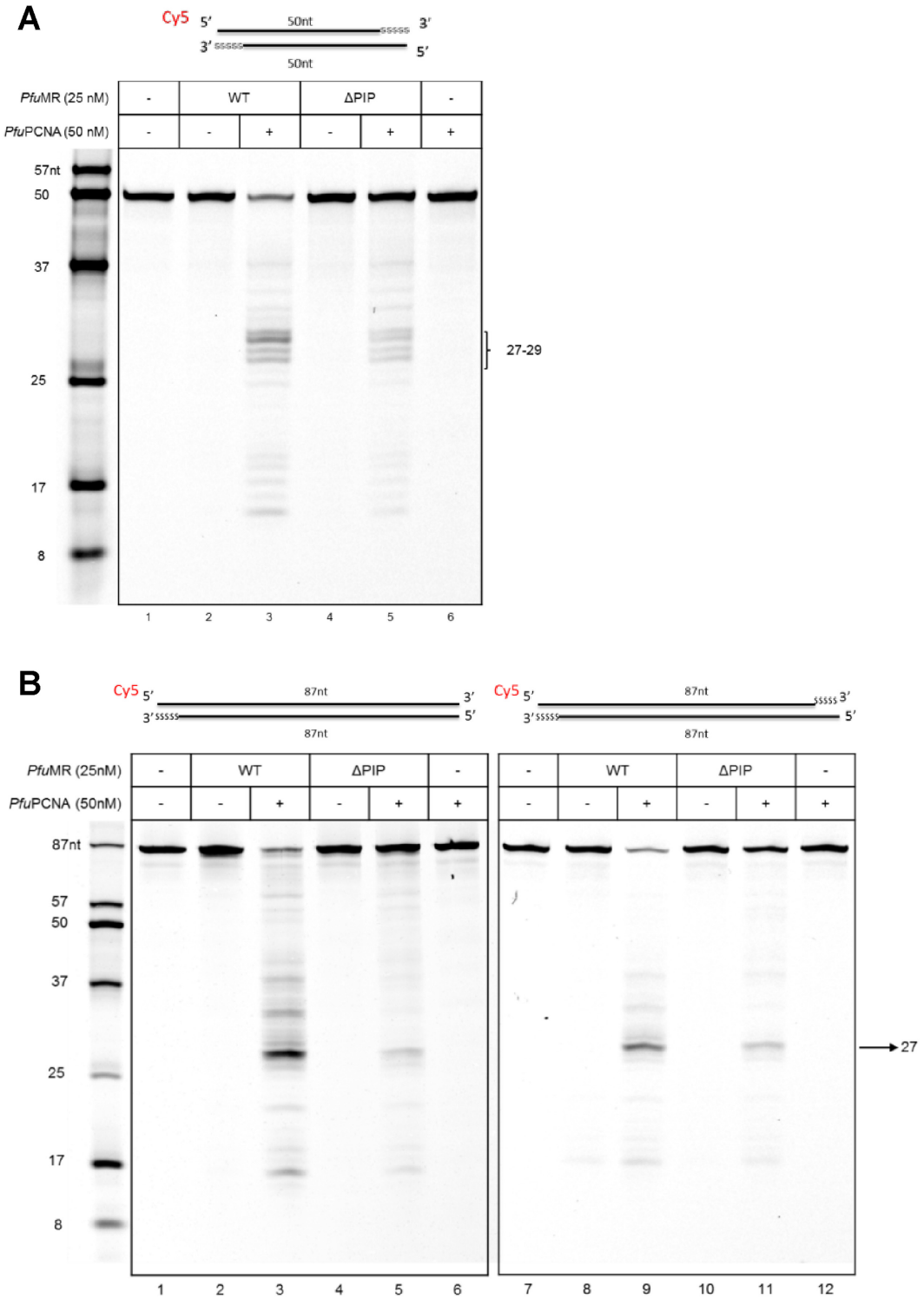

Figure 4. *Pfu*PCNA/MR interaction generates endonucleolytic cleavage at dsDNA ends. *In vitro* nuclease assays. 25 nM of DNA substrate were pre-incubated with 50 nM *Pfu*PCNA at room temperature for 5 min before adding 25 nM *Pfu*MR wt or ΔPIP. Reactions were performed for 30 min at 70°C. DNA products were resolved in 18% PAGE and fluorescence revealed using Typhoon 9500 (GE Healthcare). DNA substrates used are indicated at the top of the panels. (**A**) 50 bp DNA substrate with a phosphorothioate stretch at both 3′ ends and (**B**) 87 bp DNA substrate with protected (right panel) or unprotected (left panel) 3′ end.

Downloaded from https://academic.oup.com/nar/article-abstract/46/11/5651/4993783
by INIST-CNRS BiblioVie user
on 06 August 2018

accumulation of main products around 27–29 nt. We then asked whether a non-specific protein, such as streptavidin, bound to the 5′ end might bring about a change in cleavage pattern or efficiency. To this end, we tested a biotinylated synthetic oligonucleotide with streptavidin to block the 5′ end (Supplementary Figure S7B) and noticed no cleavage pattern difference on this particular substrate. Finally, we looked at cleavage products from 3′ end labeled substrates. The generated fragment sizes (21–23 nt) were complementary to 5′ end labeled products (27–29 nt) confirming the specificity of the endonucleolytic cut (Supplementary Figure S7C and D).

Next, we set out to examine whether there was any sequence and/or length dependence concerning the DNA substrate. To address this, we used blunt end dsDNA substrate of 87 bp that differed in sequence from the shorter substrate. Comparison of nuclease activity of the *Pfu*MR complex in presence of *Pfu*PCNA clearly showed a similar activation on this longer substrate, either blocked or accessible from the 3′ end (Figure 4B). Regardless of the size and sequence of the DNA substrates, *Pfu*PCNA stimulated the nuclease activity of the *Pfu*MR complex at the 5′ end of a DNA break to generate major 27–29 nt products through its direct interaction via the PIP-like motif. This suggests that alteration of nuclease activity by *Pfu*PCNA seems to be promiscuous and independent of length or sequences of substrates. These results are in agreement with the mechanism by which the endonuclease activity of *Pfu*Mre11 acts to incise the 5′ strand DNA close to the DSB ends (46). Taken together, these data suggest that upon association with *Pfu*PCNA, *Pfu*MR could promote endonucleolytic activity to process DNA ends.

After cleavage, the endonucleolytic product is released *via Pfu*MR/PCNA strand opening activity

Next, we investigated whether the endonucleolytic cleavage was coupled with DNA melting by the *Pfu*MR complex. As ATP-dependent DNA unwinding activity has already been reported for both prokaryotic and eukaryotic MR complexes (47–50), we made a fluorescence-based helicase assay to monitor the activity of *Pfu*MR and assess the influence of *Pfu*PCNA. We used modified S87s/87s substrate with reporter-quencher pair at the 5′ end to monitor emission of fluorescence during double strand opening in real time. To prevent partial DNA melting at high temperature, we performed unwinding assays at 55°C on the 3′ end protected substrate. In the previous cited studies (47,48,50,51), authors showed that addition of ATP/$MgCl_2$ was sufficient to detect a limited DNA unwinding activity of the MR complex. Yet, in our case, *Pfu*MR did not exhibit bona-fide DNA unwinding activity dependent on ATP/$MgCl_2$ cofactors (Figure 5A, compare lanes 1 and 4). However, in presence of *Pfu*PCNA and $MnCl_2$, conditions for which *Pfu*MR also displayed nuclease activity, strand opening activity was detected (Figure 5A, compare lanes 4 and 8). We obtained similar results with the same substrate but containing the reporter-quencher pair located at internal position 23 nt from 5′ end of the top strand (Figure 5B), indicating that local DNA melting extended from the cleavage site down to the 5′ extremity and suggesting that this DNA fragment was displaced by the *Pfu*PCNA/MR complex. To confirm this, we performed nuclease assays using the same substrates in similar conditions and resolved DNA products in native PAGE (Supplementary Figure S8). Data showed generation of a single strand DNA fragment of about 30 nt, corresponding to the displaced FAM-labeled fragment from the 5′ end. From these results, we can propose that coordination of endonuclease and local strand opening activities of *Pfu*PCNA/MR complex leads to the release of a small 5′ end ssDNA fragment to generate a DNA product with a 3′ ssDNA overhang of about 30 nt exposed.

*Pfu*PCNA does not interfere with ATP hydrolysing cycle of *Pfu*Rad50

At this point, we demonstrated that *Pfu*PCNA stimulates *Pfu*MR nuclease activity depending on ATP presence. A member of the ATP Binding Cassette (ABC) protein superfamily, Rad50 contains a conserved Nucleotide Binding Domain (NBD) that dimerizes upon two ATP molecules binding at dimer interface (45). By binding and hydrolysing ATP, Rad50 drives dynamic structural transitions of the MR complex controlling DNA unwinding and nuclease activities (49,52–56). To examine effect of the *Pfu*PCNA/MR complex interaction on ATPase activity, we measured radioactive phosphate released by ATP hydrolysis in conditions where *Pfu*MR complex was deficient in nuclease activity (without $MnCl_2$). As observed in several other studies, *Pfu*MR alone exhibited weak ATPase activity that was not stimulated by the addition of dsDNA substrate (Supplementary Figure S9). In addition, we showed that *Pfu*PCNA did not significantly regulate ATPase activity of *Pfu*MR and hence may have no effect on *Pfu*MR conformational change; similar data (not shown) were obtained in presence of $MnCl_2$.

DISCUSSION

MR complex is involved in various aspects of DSB repair, including sensing DSB triggering signal pathways and facilitating DSB repair through different pathways. Among hyperthermophilic archaea, gene deletions of *mre11* and *rad50* are lethal for cells arguing for their apparent essentiality, which distinguishes HA from all other cellular organisms, including mesophilic archaea (for a review, see (5)). Here we revealed *in vitro* physical association and functional interplay between the DNA clamp PCNA and the recombination MR complex of *P. furiosus*. To support this conclusion, we found that (i) *Pfu*MR directly interacts with *Pfu*PCNA via a PIP-like motif and (ii) *Pfu*PCNA regulates *Pfu*MR ATP-dependent nuclease activity to promote endonucleolytic cleavage about 30 nt from 5′-terminated dsDNA.

We demonstrated that PCNA binds directly to the Mre11–Rad50 complex of *P. furiosus* and that the interaction is mediated by a non-canonical PIP motif located in the C-terminal region of *Pfu*Mre11. The conspicuous difference between the *Pfu*Mre11 motif and the canonical PIP motif is the absence of the well-conserved glutamine residue. For several PCNA-interacting partners, the PIP motif contains a glutamine residue involved in multiple interactions

Downloaded from https://academic.oup.com/nar/article-abstract/46/11/5651/4993783
by INIST-CNRS BiblioVie user
on 06 August 2018

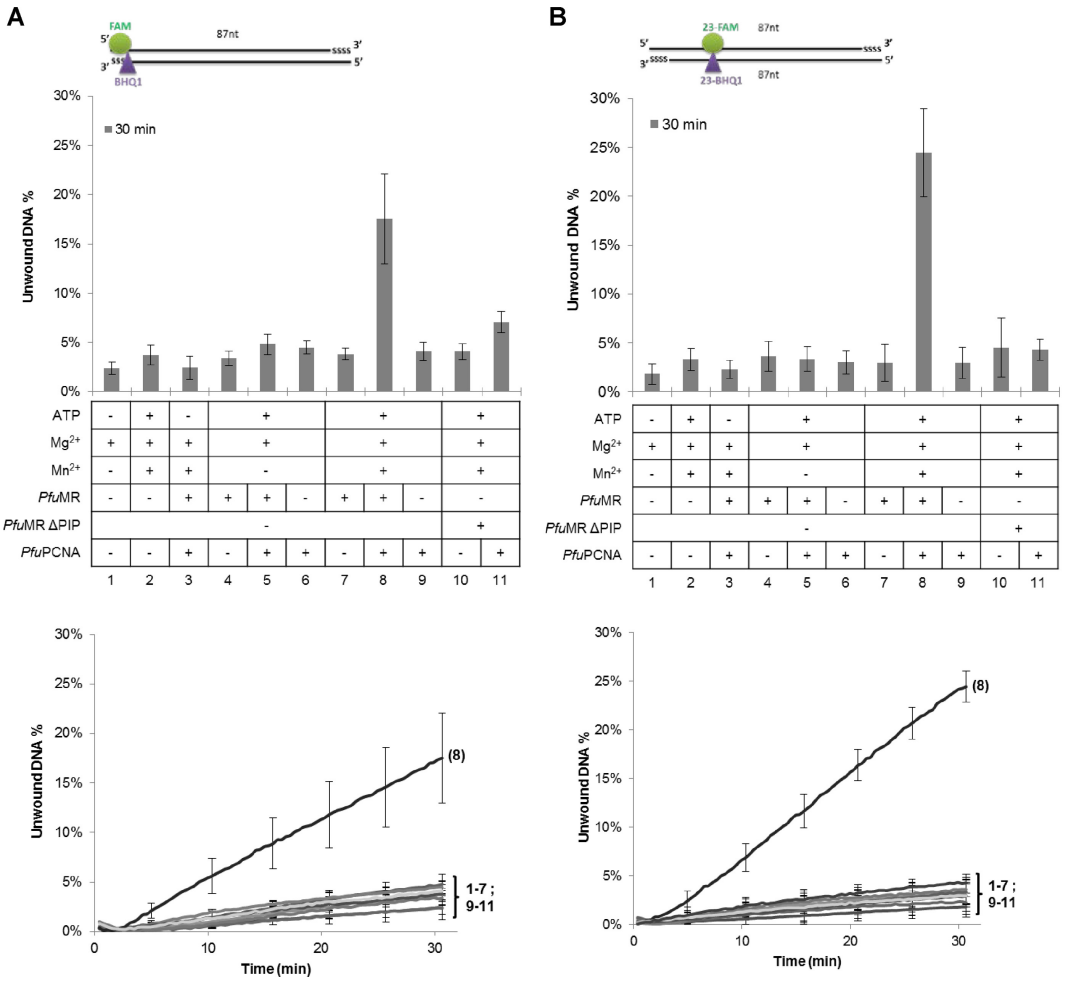

Figure 5. The endonucleolytic product from *Pfu*PCNA/MR activity is displaced from dsDNA. Results from real-time fluorescence DNA unwinding assays are presented on histogram chart with the percentage of unwound quenched substrates at 55°C after 30 min of time reaction. The dsDNA substrates used are illustrated above each histogram: RQ-S87s/87s substrate (**A**) contained a reporter-quencher pair at one extremity (+5 of the 3′ strand) consisting of dsDNA duplex; (**B**) RQ23-S87s/87s substrate had the reporter-quencher pair located at internal position 23 of dsDNA. Kinetics of DNA unwinding assays are displayed in the panels below, curves numbering corresponds to the histogram lane number (from 1 to 11). 25 nM DNA substrate were pre-incubated with 50 nM *Pfu*PCNA at room temperature for 5 min before adding 25 nM *Pfu*MR wt or ΔPIP. Reactions were performed for 30 min at 55°C in buffer with 300 mM NaCl, 5 mM $MgCl_2$ complemented with 1 mM ATP and 5 mM $MnCl_2$ as indicated in the table below histograms (see 'Materials and methods' for complete protocol). Experiments were performed in triplicate and error bars correspond to standard deviation.

with PCNA surface residues (38). Recently, a number of additional proteins that bind to PCNA have been reported (reviewed in (19–21,57)). Among them, some PCNA partners showed a PIP motif lacking this glutamine residue, and its absence has also been observed for homologue proteins, such as RFC in Archaea (58). Interestingly, the N-terminal part of the *Pfu*Mre11 peptide contains a basic region composed mainly of lysine (K) amino acids. As described for the PIP motif of RFC from *P. furiosus,* these residues could establish electrostatic interactions with the negatively charged surface of the PCNA C-terminal tail and compensate for the absence of glutamine residue (59,60). These results suggest that the peptide detected on *Pfu*Mre11 sequences is a variation on a theme of the canonical PIP motif, lacking the otherwise conserved glutamine residue, and mediates interaction between *Pfu*PCNA and the *Pfu*MR complex

Remarkably, the putative PCNA interacting motif is conserved among Mre11 sequences of all Thermococcales species and of *Archaeoglobus fulgidus*. Similar PCNA interaction motifs were not found in other archaea or in eukaryotic Mre11 sequences. However, a search for a canonical PIP motif (Q-x(2)-[LIVM]-x(2)-[FYW]-[FYWLIVM]) in generic databases Swiss-Prot and TrEMBL, using Mre11 as description filter, identified Mre11 sequences from the orders Methanosarcinales and Halobacteriales as potentially harbouring a canonical PIP motif at the extreme C-terminus region (data not shown). This suggests that the interaction between PCNA and the MR complex could be a more general feature, not only restricted to these phylogenetic branches. In addition, proteins may use additional regions to interact with the DNA clamp and novel PCNA interacting motifs have been identified since the classic PIP-box discovery (21,61). In this context, this hypothesis deserves to be tested, particularly for eukaryotic Mre11 for which a co-localisation with PCNA was observed in human during the S phase of the cell cycle (62).

Downloaded from https://academic.oup.com/nar/article-abstract/46/11/5651/4993783
by INIST-CNRS BiblioVie user
on 06 August 2018

Besides the physical interaction, we described a functional interplay between the recombination complex and *Pfu*PCNA. First, we demonstrated that *Pfu*MR is weakly active at moderate ionic strength, the condition prevailing in *P. furiosus* cells. We also demonstrated that, in these particular conditions the DNA sliding clamp stimulates and modulates nuclease activity of *Pfu*MR complex. Our data thus indicate that DNA resection initiated by *Pfu*MR could be regulated by the DNA sliding clamp. We showed that upon association with *Pfu*PCNA, the *Pfu*MR complex generates a major internal incision in the 5′ strand proximal to DSB ends. Our findings are consistent with recent study in budding yeast, wherein a distinct MR complex partner, Sae2, influenced the activity of MR in a comparable manner, by activating only the endonuclease activity of the Mre11–Rad50–Xrs2 complex (46). In addition, it was shown that the 5′ strand cleavage by eukaryotic MR was strongly enhanced by a protein block mimicking a covalently bound topoisomerase-like protein (46). While MR nuclease activities are dispensable for the resection of 'clean' DSBs (63), endonuclease activity is essential to clear obstructed DNA ends (64). Consistent with this property, we also demonstrated that *P. furiosus* MR complex was able to cleave ds break DNA intermediates with a streptavidin block at the 5′ end or with both ends blocked with phosphorothioate residues. The reported behaviour of T4 phage system gp46/47 (MR homologues) in presence of the protein factors gp32 and UvsY was also comparable to what we observed for the archaeal *Pfu*PCNA/MR complex, since the degradation profile of gp46/47 was shifted towards the generation of endonuclease products between 15 and 25 nt (30). More recently, Deshpande *et al.*, demonstrated for human proteins the role of Nbs1, the third component of the MR/N complex, in regulating MR activities by inhibiting exonuclease activity on clean ends, whereas phosphorylated CtIP, the orthologue of Sae2, stimulates endonucleolytic cleavage (65).

These different reports emphasize the importance of regulating endo- and exonuclease activities of Mre11 within the MR complex for DSB repair and that this regulation is tightly coupled with ATP-dependent conformational changes of the MR complex. A major contribution of the present study is that we revealed *Pfu*PCNA as a new interacting partner stimulating nuclease activity of the *Pfu*MR complex. The molecular mechanisms that would explain how *Pfu*PCNA triggers this internal incision by *Pfu*MR remain to be determined.

As mentioned earlier, the cycle of ATP binding and hydrolysis is associated with conformational changes of the MR complex, with transition between ATP-bound and ATP-hydrolysed states, where the ATP-bound form mediates DNA end binding, whereas ATP-hydrolyzed state renders the Mre11 nuclease active site accessible. Here, we showed that the endonucleolytic cleavage induced by the *Pfu*PCNA/MR complex is ATP-dependent, but that *Pfu*PCNA had no effect on ATP hydrolysis or DNA binding activities of *Pfu*MR. Interestingly, the PIP-like motif in *Pfu*Mre11 is located close to the RBD domain involved in binding of the Rad50 subunit. PCNA and the Rad50 subunit slide or diffuse along DNA whereas Mre11 is required for DNA end recognition and nuclease activities (66). Further structural and biochemical analysis would be required to determine if one of the two proteins has an effect on its partner's diffusion along the DNA or if *Pfu*PCNA interacts preferentially with a conformation of the *Pfu*MR complex. In support of the latter hypothesis, we showed by SPR that a more stable *Pfu*PCNA/MR complex was formed in presence of ATP, and in the case of the *Pfu*MR construct with truncated *Pfu*Rad50, the complex was faster to dissociate from *Pfu*PCNA (data not shown), indicating that the *Pfu*Rad50 coiled-coil domain also has a role in the stabilisation of the interaction. Structural determination of the *Pfu*PCNA/MR complex with DNA would be important for understanding how *Pfu*PCNA controls or binds a specific conformational state of *Pfu*MR complex.

According to bidirectional resection model of DNA DSB, upon the initial endonuclease cleavage, the Mre11 exonuclease proceeds back towards the DNA end *via* its 3′→5′ exonuclease activity (model discussed in (32,67). Astonishingly, in our results no 5′-products shorter than 15 nt were observed in the nuclease assays, suggesting an absence of extensive 3′→5′ resection for the second step. The most likely explanation for this observation is that archaeal *Pfu*MR displaced the 5′ end through a combination of melting and endonuclease activities. This explanation is consistent with the reported ability of the eukaryotic MR(N/X) complex to open the DNA helix on ∼20 base pairs at the end of the duplex in an ATP-dependent manner (47,50).

In our conditions, the *Pfu*PCNA/MR complex did not display genuine DNA helicase activity dependent on ATP and Mg^{2+}. To date, ATP-dependent DNA unwinding activity has only been reported for bacterial MR and eukaryotic MRN complexes. This finding suggests that this unwinding activity is not conserved in the archaeal MR complex. However, in conditions suitable for DNA cleavage, the 5′ labeled product (27–29 nt) was displaced from the initial dsDNA substrate. We thus propose that *Pfu*PCNA stimulates *Pfu*MR DNA end processing leading to an internal cleavage coupled with 5′ end removal. As described by Liu and collaborators, ATP-dependent DNA melting facilitates the access of Mre11 for DNA cleavage (49). Here, we cannot elucidate which, from the cleavage or the DNA opening event, occurs first. Altogether, we assume that the short-range processing by *Pfu*PCNA/MR would generate 3′-tailed substrate that could be suitable for additional partners responsible for extended resection. The helicase/nuclease HerA/NurA complex was found in all thermophilic archaea, clustered in the operon encoding Mre11 and Rad50 (68), and *in vitro* experiments demonstrated that Rad50, Mre11, HerA and NurA co-operate for resection of the 5′ strand at a DNA double strand break, generating a 3′ ssDNA suitable for the recombinase RadA (42). In *Pyrococcus abyssi,* at least 20 nt are required to bind one RPA trimer onto DNA efficiently (unpublished data). Here, the *Pfu*PCNA/MR interplay generates a 3′ overhang of 27–29 nt suitable for RPA loading and thus for 3′ tail protection from degradation by NurA, while the complex HerA/NurA can still extend 5′ strand resection. Taken together, our findings indicate that *Pfu*MR interacts with *Pfu*PCNA physically and functionally in a manner consistent with an end resection process for the HR pathway.

Downloaded from https://academic.oup.com/nar/article-abstract/46/11/5651/4993783
by INIST-CNRS BiblioVie user
on 06 August 2018

This study leads to questions about the role of PCNA/MR interplay in hyperthermophilic archaea. The precise employment of the different process components in cases of either DSB damage or replication fork stalling remains to be clarified. Deciphering the role of PCNA/MR interplay in HA will require further genetic and structural studies, with the hope that it might provide clues to improve understanding of recombinational repair processes in archaea.

SUPPLEMENTARY DATA

Supplementary Data are available at NAR Online.

ACKNOWLEDGEMENTS

We thank Tanya Paull, John Tainer and Bernard Connolly for sending clones and we are grateful to Gareth Williams for providing proteins and for helpful discussions.
Author Contributions: G.H., L.Y., S.L., E.H., B.C.O., D.F. designed the experiments; G.H., Y.L., S.L., R.D., D.K.P., A.B., P.F.P. performed the experiments; G.H., D.F., Y.L., S.L. analysed the data; G.H., D.F., Y.L. wrote the paper; and D.F. conceived and directed the study.

FUNDING

Ifremer; CNRS; University of Western Britany. This work was supported by the French "Agence Nationale pour la Recherche" [ANR-16-CE12-0016 to B.C.O. and D.F.]. Funding for open access charge: Ifremer.
Conflict of interest statement. None declared.

REFERENCES

1. Gerard,E., Jolivet,E., Prieur,D. and Forterre,P. (2001) DNA protection mechanisms are not involved in the radioresistance of the hyperthermophilic archaea Pyrococcus abyssi and P. furiosus. *Mol. Genet. Genomics*, **266**, 72–78.
2. Peak,M.J., Robb,F.T. and Peak,J.G. (1995) Extreme resistance to thermally induced DNA backbone breaks in the hyperthermophilic archaeon Pyrococcus furiosus. *J. Bacteriol.*, **177**, 6316–6318.
3. Larmony,S., Garnier,F., Hoste,A. and Nadal,M. (2015) A specific proteomic response of Sulfolobus solfataricus P2 to gamma radiations. *Biochimie*, **118**, 270–277.
4. Kelman,L.M. and Kelman,Z. (2014) Archaeal DNA replication. *Annu. Rev. Genet.*, **48**, 71–97.
5. Grogan,D.W. (2015) Understanding DNA repair in hyperthermophilic Archaea: persistent gaps and other reasons to focus on the fork. *Archaea*, **2015**, 942605.
6. Shiraishi,M., Ishino,S., Yamagami,T., Egashira,Y., Kiyonari,S. and Ishino,Y. (2015) A novel endonuclease that may be responsible for damaged DNA base repair in Pyrococcus furiosus. *Nucleic Acids Res.*, **43**, 2853–2863.
7. Giroux,X. and MacNeill,S.A. (2016) A novel archaeal DNA repair factor that acts with the UvrABC system to repair mitomycin C-induced DNA damage in a PCNA-dependent manner. *Mol. Microbiol.*, **99**, 1–14.
8. Tori,K., Ishino,S., Kiyonari,S., Tahara,S. and Ishino,Y. (2013) A novel Single-Strand specific 3′-5′ exonuclease found in the hyperthermophilic archaeon, pyrococcus furiosus. *PLoS One*, **8**, e58497.
9. Li,Z., Pan,M., Santangelo,T.J., Chemnitz,W., Yuan,W., Edwards,J.L., Hurwitz,J., Reeve,J.N. and Kelman,Z. (2011) A novel DNA nuclease is stimulated by association with the GINS complex. *Nucleic Acids Res.*, **39**, 6114–6123.
10. Li,Z., Santangelo,T.J., Cubonova,L., Reeve,J.N. and Kelman,Z. (2010) Affinity purification of an archaeal DNA replication protein network. *MBio*, **1**, e00221.
11. Ren,B., Kuhn,J., Meslet-Cladiere,L., Briffotaux,J., Norais,C., Lavigne,R., Flament,D., Ladenstein,R. and Myllykallio,H. (2009) Structure and function of a novel endonuclease acting on branched DNA substrates. *EMBO J.*, **28**, 2479–2489.
12. Meslet-Cladiere,L., Norais,C., Kuhn,J., Briffotaux,J., Sloostra,J.W., Ferrari,E., Hubscher,U., Flament,D. and Myllykallio,H. (2007) A novel proteomic approach identifies new interaction partners for proliferating cell nuclear antigen. *J. Mol. Biol.*, **372**, 1137–1148.
13. Guy,C.P. and Bolt,E.L. (2005) Archaeal Hel308 helicase targets replication forks in vivo and in vitro and unwinds lagging strands. *Nucleic Acids Res.*, **33**, 3678–3690.
14. Fujikane,R., Komori,K., Shinagawa,H. and Ishino,Y. (2005) Identification of a novel helicase activity unwinding branched DNAs from the hyperthermophilic archaeon, Pyrococcus furiosus. *J. Biol. Chem.*, **280**, 12351–12358.
15. Pluchon,P.F., Fouqueau,T., Creze,C., Laurent,S., Briffotaux,J., Hogrel,G., Palud,A., Henneke,G., Godfroy,A., Hausner,W. *et al.* (2013) An extended network of genomic maintenance in the archaeon pyrococcus abyssi highlights unexpected associations between eucaryotic homologs. *PLoS One*, **8**, e79707.
16. Henneke,G., Gueguen,Y., Flament,D., Azam,P., Querellou,J., Dietrich,J., Hubscher,U. and Raffin,J.P. (2002) Replication factor C from the hyperthermophilic archaeon Pyrococcus abyssi does not need ATP hydrolysis for clamp-loading and contains a functionally conserved RFC PCNA-binding domain. *J. Mol. Biol.*, **323**, 795–810.
17. Cann,I.K., Ishino,S., Hayashi,I., Komori,K., Toh,H., Morikawa,K. and Ishino,Y. (1999) Functional interactions of a homolog of proliferating cell nuclear antigen with DNA polymerases in Archaea. *J. Bacteriol.*, **181**, 6591–6599.
18. Maga,G. and Hubscher,U. (2003) Proliferating cell nuclear antigen (PCNA): a dancer with many partners. *J. Cell Sci.*, **116**, 3051–3060.
19. Pan,M., Kelman,L.M. and Kelman,Z. (2011) The archaeal PCNA proteins. *Biochem. Soc. Trans.*, **39**, 20–24.
20. Moldovan,G.L., Pfander,B. and Jentsch,S. (2007) PCNA, the maestro of the replication fork. *Cell*, **129**, 665–679.
21. Gilljam,K.M., Feyzi,E., Aas,P.A., Sousa,M.M., Muller,R., Vagbo,C.B., Catterall,T.C., Liabakk,N.B., Slupphaug,G., Drablos,F. *et al.* (2009) Identification of a novel, widespread, and functionally important PCNA-binding motif. *J. Cell Biol.*, **186**, 645–654.
22. Stracker,T.H. and Petrini,J.H. (2011) The MRE11 complex: starting from the ends. *Nat. Rev. Mol. Cell Biol.*, **12**, 90–103.
23. Daley,J.M., Niu,H., Miller,A.S. and Sung,P. (2015) Biochemical mechanism of DSB end resection and its regulation. *DNA Repair*, **32**, 66–74.
24. Goodarzi,A.A. and Jeggo,P.A. (2013) The repair and signaling responses to DNA double-strand breaks. *Adv. Genet.*, **82**, 1–45.
25. White,M.F. (2011) Homologous recombination in the archaea: the means justify the ends. *Biochem. Soc. Trans.*, **39**, 15–19.
26. Huertas,P. (2010) DNA resection in eukaryotes: deciding how to fix the break. *Nat. Struct. Mol. Biol.*, **17**, 11–16.
27. Bartlett,E.J., Brissett,N.C. and Doherty,A.J. (2013) Ribonucleolytic resection is required for repair of strand displaced nonhomologous end-joining intermediates. *PNAS*, **110**, E1984–E1991.
28. Fujikane,R., Ishino,S., Ishino,Y. and Forterre,P. (2010) Genetic analysis of DNA repair in the hyperthermophilic archaeon, Thermococcus kodakaraensis. *Genes Genet. Syst.*, **85**, 243–257.
29. Huang,Q., Liu,L., Liu,J., Ni,J., She,Q. and Shen,Y. (2015) Efficient 5′-3′ DNA end resection by HerA and NurA is essential for cell viability in the crenarchaeon Sulfolobus islandicus. *BMC Mol. Biol.*, **16**, 2.
30. Herdendorf,T.J., Albrecht,D.W., Benkovic,S.J. and Nelson,S.W. (2011) Biochemical characterization of bacteriophage T4 Mre11–Rad50 complex. *J. Biol. Chem.*, **286**, 2382–2392.
31. Lafrance-Vanasse,J., Williams,G.J. and Tainer,J.A. (2015) Envisioning the dynamics and flexibility of Mre11–Rad50-Nbs1 complex to decipher its roles in DNA replication and repair. *Progr. Biophys. Mol. Biol.*, **117**, 182–193.
32. Paull,T.T. (2010) Making the best of the loose ends: Mre11/Rad50 complexes and Sae2 promote DNA double-strand break resection. *DNA Repair*, **9**, 1283–1291.

Downloaded from https://academic.oup.com/nar/article-abstract/46/11/5651/4993783
by INIST-CNRS BiblioVie user
on 06 August 2018

33. Emptage,K., O'Neill,R., Solovyova,A. and Connolly,B.A. (2008) Interplay between DNA polymerase and proliferating cell nuclear antigen switches off base excision repair of uracil and hypoxanthine during replication in archaea. *J. Mol. Biol.*, **383**, 762–771.
34. Hopfner,K.P., Karcher,A., Shin,D., Fairley,C., Tainer,J.A. and Carney,J.P. (2000) Mre11 and Rad50 from Pyrococcus furiosus: cloning and biochemical characterization reveal an evolutionarily conserved multiprotein machine. *J. Bacteriol.*, **182**, 6036–6041.
35. Williams,G.J., Williams,R.S., Williams,J.S., Moncalian,G., Arvai,A.S., Limbo,O., Guenther,G., SilDas,S., Hammel,M., Russell,P. *et al.* (2011) ABC ATPase signature helices in Rad50 link nucleotide state to Mre11 interface for DNA repair. *Nat. Struct. Mol. Biol.*, **18**, 423–431.
36. Winter,J.A. and Bunting,K.A. (2012) Rings in the extreme: PCNA interactions and adaptations in the archaea. *Archaea*, **2012**, 951010.
37. Warbrick,E. (1998) PCNA binding through a conserved motif. *Bioessays*, **20**, 195–199.
38. Gulbis,J.M., Kelman,Z., Hurwitz,J., ODonnell,M. and Kuriyan,J. (1996) Structure of the C-terminal region of p21(WAF1/CIP1) complexed with human PCNA. *Cell*, **87**, 297–306.
39. Fujikane,R., Shinagawa,H. and Ishino,Y. (2006) The archaeal Hjm helicase has recQ-like functions, and may be involved in repair of stalled replication fork. *Genes Cells*, **11**, 99–110.
40. Creze,C., Ligabue,A., Laurent,S., Lestini,R., Laptenok,S.P., Khun,J., Vos,M.H., Czjzek,M., Myllykallio,H. and Flament,D. (2012) Modulation of the Pyrococcus abyssi NucS endonuclease activity by replication clamp at functional and structural levels. *J. Biol. Chem.*, **287**, 15648–15660.
41. Hasan,M.N., Hagedoorn,P.L. and Hagen,W.R. (2002) Pyrococcus furiosus ferredoxin is a functional dimer. *FEBS Lett.*, **531**, 335–338.
42. Hopkins,B.B. and Paull,T.T. (2008) The P. furiosus mre11/rad50 complex promotes 5′ strand resection at a DNA double-strand break. *Cell*, **135**, 250–260.
43. Hopfner,K.P., Karcher,A., Craig,L., Woo,T.T., Carney,J.P. and Tainer,J.A. (2001) Structural biochemistry and interaction architecture of the DNA double-strand break repair Mre11 nuclease and Rad50-ATPase. *Cell*, **105**, 473–485.
44. Paull,T.T. and Gellert,M. (1998) The 3′ to 5′ exonuclease activity of Mre 11 facilitates repair of DNA double-strand breaks. *Mol. Cell*, **1**, 969–979.
45. Hopfner,K.P., Karcher,A., Shin,D.S., Craig,L., Arthur,L.M., Carney,J.P. and Tainer,J.A. (2000) Structural biology of Rad50 ATPase: ATP-driven conformational control in DNA double-strand break repair and the ABC-ATPase superfamily. *Cell*, **101**, 789–800.
46. Cannavo,E. and Cejka,P. (2014) Sae2 promotes dsDNA endonuclease activity within Mre11–Rad50-Xrs2 to resect DNA breaks. *Nature*, **514**, 122–125.
47. Cannon,B., Kuhnlein,J., Yang,S.H., Cheng,A., Schindler,D., Stark,J.M., Russell,R. and Paull,T.T. (2013) Visualization of local DNA unwinding by Mre11/Rad50/Nbs1 using single-molecule FRET. *PNAS*, **514**, 122–125.
48. Chen,L., Trujillo,K.M., Van Komen,S., Roh,D.H., Krejci,L., Lewis,L.K., Resnick,M.A., Sung,P. and Tomkinson,A.E. (2005) Effect of amino acid substitutions in the rad50 ATP binding domain on DNA double strand break repair in yeast. *J. Biol. Chem.*, **280**, 2620–2627.
49. Liu,Y., Sung,S., Kim,Y., Li,F., Gwon,G., Jo,A., Kim,A.K., Kim,T., Song,O.K., Lee,S.E. *et al.* (2016) ATP-dependent DNA binding, unwinding, and resection by the Mre11/Rad50 complex. *EMBO J.*, **35**, 743–758.
50. Paull,T.T. and Gellert,M. (1999) Nbs1 potentiates ATP-driven DNA unwinding and endonuclease cleavage by the Mre11/Rad50 complex. *Gene Dev.*, **13**, 1276–1288.
51. Liu,Y., Sung,S., Kim,Y., Li,F., Gwon,G., Jo,A., Kim,A.K., Kim,T., Song,O.K., Lee,S.E. *et al.* (2016) ATP-dependent DNA binding, unwinding, and resection by the Mre11/Rad50 complex. *EMBO J.*, **35**, 743–758.
52. Deshpande,R.A., Williams,G.J., Limbo,O., Williams,R.S., Kuhnlein,J., Lee,J.H., Classen,S., Guenther,G., Russell,P., Tainer,J.A. *et al.* (2014) ATP-driven Rad50 conformations regulate DNA tethering, end resection, and ATM checkpoint signaling. *EMBO J.*, **33**, 482–500.
53. Mockel,C., Lammens,K., Schele,A. and Hopfner,K.P. (2012) ATP driven structural changes of the bacterial Mre11:Rad50 catalytic head complex. *Nucleic Acids Res.*, **40**, 914–927.
54. Majka,J., Alford,B., Ausio,J., Finn,R.M. and McMurray,C.T. (2011) ATP hydrolysis by RAD50 protein switches MRE11 enzyme from endonuclease to exonuclease. *J. Biol. Chem.*, **287**, 2328–2341.
55. Lim,H.S., Kim,J.S., Park,Y.B., Gwon,G.H. and Cho,Y. (2011) Crystal structure of the Mre11–Rad50-ATPgammaS complex: understanding the interplay between Mre11 and Rad50. *Gene Dev.*, **25**, 1091–1104.
56. Lammens,K., Bemeleit,D.J., Mockel,C., Clausing,E., Schele,A., Hartung,S., Schiller,C.B., Lucas,M., Angermuller,C., Soding,J. *et al.* (2011) The Mre11:Rad50 structure shows an ATP-Dependent molecular Clamp in DNA Double-Strand break repair. *Cell*, **145**, 54–66.
57. Pedley,A.M., Lill,M.A. and Davisson,V.J. (2014) Flexibility of PCNA-Protein interface accommodates differential binding partners. *PLoS One*, **9**, e102481.
58. Warbrick,E. (2000) The puzzle of PCNA's many partners. *Bioessays*, **22**, 997–1006.
59. Matsumiya,S., Ishino,Y. and Morikawa,K. (2001) Crystal structure of an archaeal DNA sliding clamp: proliferating cell nuclear antigen from Pyrococcus furiosus. *Protein Sci.*, **10**, 17–23.
60. Matsumiya,S., Ishino,S., Ishino,Y. and Morikawa,K. (2002) Physical interaction between proliferating cell nuclear antigen and replication factor C from Pyrococcus furiosus. *Genes Cells*, **7**, 911–922.
61. Xu,H., Zhang,P., Liu,L. and Lee,M.Y. (2001) A novel PCNA-binding motif identified by the panning of a random peptide display library. *Biochemistry*, **40**, 4512–4520.
62. Maser,R.S., Mirzoeva,O.K., Wells,J., Olivares,H., Williams,B.R., Zinkel,R.A., Farnham,P.J. and Petrini,J.H. (2001) Mre11 complex and DNA replication: linkage to E2F and sites of DNA synthesis. *J. Mol. Cell Biol.*, **21**, 6006–6016.
63. Llorente,B. and Symington,L.S. (2004) The Mre11 nuclease is not required for 5′ to 3′ resection at multiple HO-induced double-strand breaks. *J. Mol. Cell Biol.*, **24**, 9682–9694.
64. Shibata,A., Moiani,D., Arvai,A.S., Perry,J., Harding,S.M., Genois,M.M., Maity,R., van Rossum-Fikkert,S., Kertokalio,A., Romoli,F. *et al.* (2013) DNA double-strand break repair pathway choice is directed by distinct MRE11 nuclease activities. *Mol. Cell*, **53**, 7–18.
65. Deshpande,R.A., Lee,J.H., Arora,S. and Paull,T.T. (2016) Nbs1 converts the human Mre11/Rad50 nuclease complex into an Endo/Exonuclease machine specific for protein–DNA adducts. *Mol. Cell*, **64**, 593–606.
66. Myler,L.R., Gallardo,I.F., Soniat,M.M., Deshpande,R.A., Gonzalez,X.B., Kim,Y., Paull,T.T. and Finkelstein,I.J. (2017) Single-Molecule imaging reveals how Mre11–Rad50-Nbs1 initiates DNA break repair. *Molecular Cell*, **67**, 891–898.
67. Cejka,P. (2015) DNA end resection: nucleases team up with the right partners to initiate homologous recombination. *J. Biol. Chem.*, **290**, 22931–22938.
68. Constantinesco,F., Forterre,P. and Elie,C. (2002) NurA, a novel 5′ -3′ nuclease gene linked to rad50 and mre11 homologs of thermophilic Archaea. *Embo Rep*, **3**, 537–542.

Downloaded from https://academic.oup.com/nar/article-abstract/46/11/5651/4993783
by INIST-CNRS BiblioVie user
on 06 August 2018